J. Fluid Mech. (2009), *vol.* 641, *pp.* 63–84.
doi:10.1017/S0022112009991546

Flow regimes for the immiscible liquid–liquid displacement in capillary tubes with complete wetting of the displaced liquid

EDSON J. SOARES[1] AND RONEY L. THOMPSON[2]†

[1]LFTC, Department of Mechanical Engineering, Universidade Federal do Espirito Santo, Avenida Fernando Ferrari, 514, Goiabeiras, 29075-910 ES, Brazil

[2]LFTC-LMTA, Department of Mechanical Engineering (PGMEC), Universidade Federal Fluminense, Rua Passo da Patria 156, 24210-240 Niteroi, RJ, Brazil

(Received 19 February 2009; revised 6 August 2009; accepted 7 August 2009)

The motion of two immiscible liquids in a capillary tube is analysed, theoretically and numerically, for the case in which a residual film confines the displacing liquid to the core of this tube. The theoretical analysis has shown that the three flow regimes predicted by Taylor (*J. Fluid Mech.*, vol. 10, 1961, pp. 161–165), for the case of gas-displacement, can only be achieved when the ratio of the viscosity of the displaced fluid to that of the displacing one is greater than 2. An elliptic mesh generation technique, coupled with the Galerkin finite-element method, is used to compute the velocity field and the configuration of the interface between the two fluids. A map of cases in the Cartesian space defined by the capillary number (Ca) and the viscosity ratio (N_μ) is constructed in order to locate the different flow patterns the problem exhibits. The critical capillary number at which the flow enters the transition range between the bypass regime and the full-recirculating one is given. While a decrease of the fraction of mass attached to the wall is achieved by decreasing Ca or increasing N_μ, bypass flow patterns are formed as a consequence of high values of the capillary number and viscosity ratio.

Key words: capillary flows, core-annular flows, Hele-Shaw/porous media

1. Introduction

The present work investigates the liquid–liquid displacement when a residual liquid film of the displaced fluid is formed near the wall. An important application is in oil recovery from porous media, where the liquid film of the displaced oil that remains attached to the rocks has a significance in the efficiency of the recovery during water-flooding operation. Typically, because of the high viscosity levels and slow displacement velocities involved, these kind of processes occur with negligible inertial effects. Besides that, as a consequence of the small length scale, the capillary forces play a fundamental role in the physics of the phenomena.

Figure 1 shows a scheme of the problem analysed. The tube is initially occupied by Phase 2 (generally a liquid) when Phase 1 (another liquid or a gas) is injected, forming a two-phase flow. As an idealized model, Phase 1 forms a long drop that displaces Phase 2, leaving behind a residual layer of fluid attached to the wall. When inertia is negligible, this front moves with a constant velocity U, and the configuration of the

† Email address for correspondence: rthompson@mec.uff.br

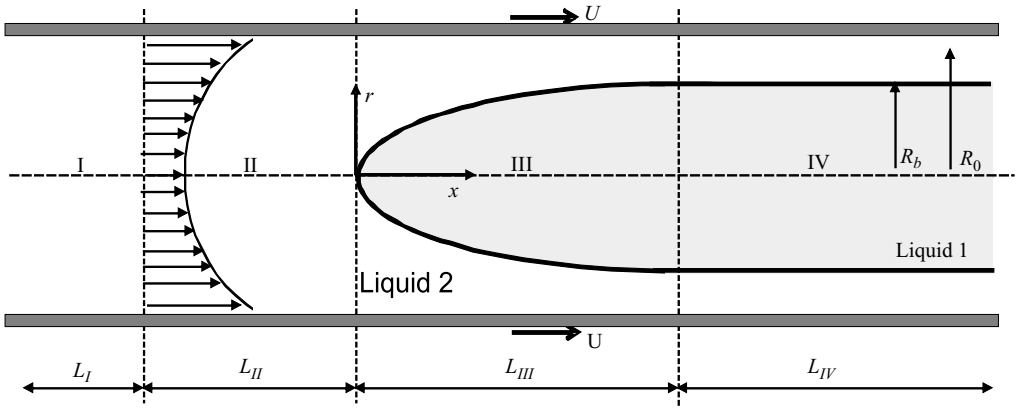

FIGURE 1. Schematics of the analysed problem.

interface achieves a fixed shape with a constant width of residual layer far enough from the tip of the drop.

Following the pioneering works carried out by Fairbrother & Stubbs (1935), Bretherton (1961), Taylor (1961) and Cox (1962), several investigators have analysed the residual liquid film that remains attached to the wall for the case of the displacement of a viscous liquid in a capillary tube when Phase 1, the displacing fluid, is a gas. The fraction of mass remaining attached to the wall, m, is defined as

$$m = 1 - \frac{R_b^2}{R_0^2}, \tag{1.1}$$

where R_0 is the radius of the tube and R_b is the radius of the drop when it has reached its constant value, as seen in figure 1. When inertial effects can be neglected, the dimensionless parameter that governs this problem is the capillary number $Ca \equiv (\mu_2 U)/\sigma$ that signifies the relative importance of viscous stresses to interfacial-tension stresses.

The experimental investigation carried out by Taylor (1961) for the problem of a gas displacing a viscous liquid is remarkable and very relevant in the context of the present work. After a co-ordinate transformation that attaches the reference frame to the tip of the bubble, he sketched three possible flow regimes of the liquid near the interface, as shown in figure 2. The first regime, figure 2(a), has a stagnation point at the tip of the bubble. It is a bypass flow, which would occur for high capillary numbers. In this case Phase 2 would pass completely and no recirculation would be formed in the displaced liquid near the free surface. The second regime occurs when another stagnation point is formed at a certain position of the centreline in the liquid domain, away from the bubble, as shown in figure 2(b). In this case, a recirculation pattern is developed. Upstream of this new stagnation point a filament at the centreline moves away from the bubble, while downstream of this point a filament at the centreline moves towards the bubble. The third flow pattern, as depicted in figure 2(c), is generally referred to a full-recirculation regime. The recirculation of Phase 2 reaches the interface with Phase 1, and thus, besides the stagnation point at the tip of the bubble, a stagnation ring at the surface is formed. It is worth noticing that there is a critical value for the fraction of mass attached to the wall, m_c, above which the flow is always in the bypass regime. For a gas displacing a Newtonian liquid, $m_c = 0.5$ (Taylor 1961).

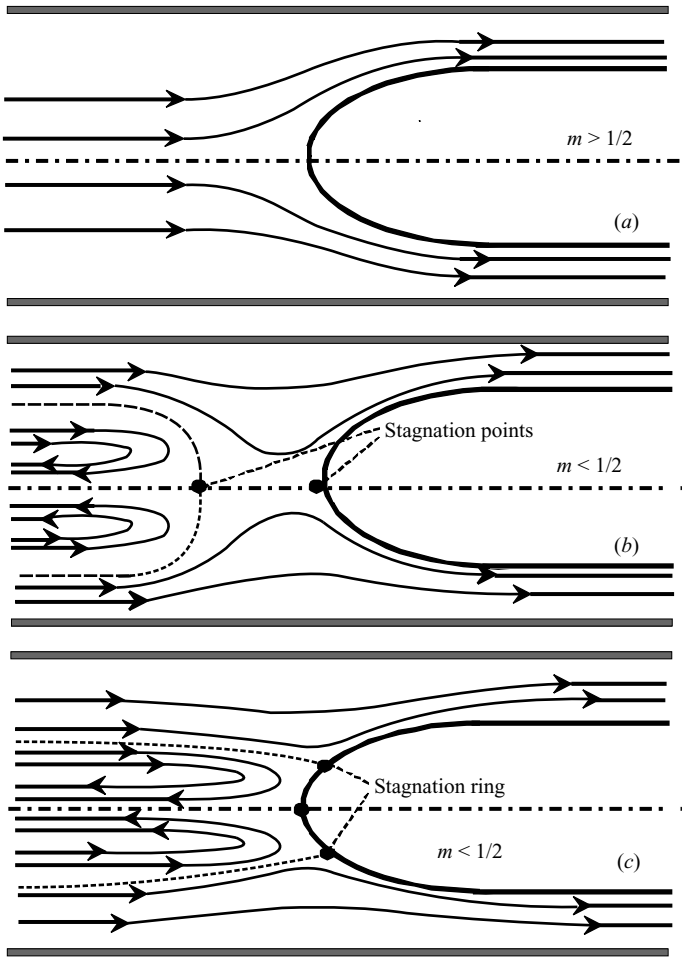

FIGURE 2. Streamline patterns suggested by Taylor for the gas-displacement in capillary tubes' problem: (*a*) bypass flow regime; (*b*) transition flow regime; and (*c*) recirculation flow regime.

Recently, some interesting literature on gas-displacement dealt with displacement of non-Newtonian liquids, as investigated in Sousa *et al.* (2007), Dimakopoulos & Tsamopoulos (2003*b*, 2004, 2007), de Souza Mendes *et al.* (2007), Sousa, Pinto & Campos (2006), Soares, Carvalho & de Souza Mendes (2006), Lee, Shaqfeh & Khomami (2002) and Huzyak & Koelling (1997), among others. In these cases, in addition to *Ca*, other dimensionless parameters related to the rheology of the displaced liquid were taken into account. These analyses gave further insights into understanding, in the problem considered, how capillary forces interact with other phenomena of complex materials, such as pseudo-plasticity, viscoplasticity and viscoelasticity. Concerning pseudo-plasticity and viscoplasticity, these works agree in the conclusion that as the displaced fluid departs from Newtonian behaviour, the fraction of the mass deposited on the tube wall decreases and the shape of the interface becomes flatter. The viscoelastic case is a little more complex. The results related to Boger-like fluids, e.g. Huzyak & Koelling (1997), indicate an increase in the residual mass fraction, while for shear-thinning fluids such as FENE-P (Lee *et al.* 2002) and PTT (Dimakopoulos & Tsamopoulos 2004) there is a competition

between pseudo-plasticity and elasticity, and therefore, for low Weissenberg numbers, gas-displacement of viscoelastic fluids can exhibit a thinner layer of deposited mass. In the context of flow regimes, Sousa *et al.* (2007) found an interesting new flow pattern with a small recirculation near the bubble for viscoplastic and pseudo-plastic materials. In this case, upstream of the second stagnation point a material filament at the centreline moves 'towards' the bubble. This flow pattern was sketched by Hodges, Jenseng & Rallison (2004) in the liquid–liquid displacement for very low capillary numbers.

It seems that the first investigation of the liquid–liquid displacement in a capillary tube was done by Goldsmith & Mason (1963). They conducted an experimental analysis adding another dimensionless parameter (besides Ca) to the problem: the ratio of viscosity of the displaced fluid to that of the displacing one, $N_\mu \equiv \mu_2/\mu_1$. In their experiments, the displacing material was, therefore, a long drop of a viscous liquid, immiscible to the liquid that was previously in the tube. They were also interested in the amount of the displaced liquid left on the tube wall as a function of N_μ and Ca. The results showed that m increases as the viscosity ratio is decreased. This trend agrees with the theoretical predictions and experimental data presented by Soares, Carvalho & de Souza Mendes (2005). Westborg & Hassager (1989) and Martinez & Udell (1990) numerically analysed the problem of the creeping flow of closed drops in a capillary tube. They found a secondary recirculation inside the drop that disappears for high capillary numbers. Martinez & Udell (1990) showed that when the undeformed drop radius is greater than 1.1 times the tube radius, the drop can be considered long. Hodges *et al.* (2004) extended Bretherton's (1961) work for the liquid–liquid displacement in the $Ca \ll 1$ limit. They found a non-monotonic behaviour for film thickness as the viscosity ratio decreases from infinity. Allouche, Frigaard & Sona (2000) investigated the displacement of two viscoplastic materials in a plane channel for the case in which interfacial tension stresses are negligible. They were interested in the process of mud removal during the primary cementing of an oil well where the fluids involved are typically non-Newtonian with viscoplastic properties. Their predictions for the yield-stress effect on the liquid film attached to the wall agrees qualitatively with the experimental results obtained by Poslinski, Oehler & Stokes (1995), who reported an experimental gas-assisted displacement in tubes for two samples of viscoplastic materials. Also, the analysis of Allouche *et al.* (2000) is in agreement with the recent numerical analysis presented by Sousa *et al.* (2007) and Dimakopoulos & Tsamopoulos (2007). Soares, Carvalho & de Souza Mendes (2008) experimentally investigated the effect of viscoelasticity on the liquid–liquid displacement and found that, within the covered range, the fraction of mass deposited at the wall is higher when viscoelastic Boger-like fluid is displaced by a Newtonian one when compared with a Newtonian–Newtonian displacement. As discussed previously, this result follows the same trend as the gas-viscoelastic Boger-like displacement.

The problems in which capillary forces are relevant to the analysis require numerical schemes that can accurately determine the configuration of the interface, since the force generated by the interfacial tension is a function of the mean radius of curvature. Compared to the gas–liquid case, the liquid–liquid displacement significantly increases the numerical efforts necessary to simulate this kind of problem. One additional complexity is due to the fact that in the gas–liquid displacement the effects of the displacing fluid (gas) are introduced into the the problem as a boundary condition, while in the liquid–liquid displacement the conservation equations have to be solved in the displacing fluid domain also. Another complexity comes from the force balance

at the interface, since in a liquid–liquid displacement case, the normal stress at the interface at the displacing-fluid side is not solely given by the pressure. For the reasons indicated above, there are few papers dealing with the analysis of the liquid–liquid displacement that consider a residual liquid film attached to the wall and include interfacial tension.

In the present paper we study the liquid–liquid displacement in a capillary tube from a purely theoretical and a numerical point of view. The theoretical analysis has led to important guidelines in the conduction of the numerical experiments and in the interpretation of the observed phenomena. We employed an elliptic grid generation methodology via a Galerkin finite-element method. The main objective of the numerical approach is to investigate the flow patterns at the liquid–liquid interface.

2. Problem formulation

The flow near the liquid–liquid interface is analysed using a moving frame of reference attached to the tip of the drop. A basic assumption of this analysis is that the configuration of the interface converges to a fixed shape and a long drop of Liquid 1 is formed. This assumption is a fairly good approximation, since inertia is neglected and the drop is not accelerating. Relative to the reference frame adopted, the capillary tube wall moves with the interface velocity U while the interface is stationary, as shown in figure 1. We are adopting this reference and the motion experienced by the part of Liquid 2 which is in contact with the wall to designate the upstream and downstream regions of the flow. In the laboratory frame, where the problem is transient, the imposed conditions are, generally, the inlet and outlet pressures, and therefore, the front velocity U is a consequence of this input. Since U is an imposed condition in the present approach, the translational invariance of the problem is taken into account in the numerical method by letting the pressure at the outlet free. The reason why it is preferred to let the outlet pressure free than the inlet one is because the pressure jump between the two fluids at the outlet is unknown *a priori*. In this case, the location of tip of the interface is not fixed but is determined by the level of the inlet pressure. The problem is considered axisymmetric with vanishing azimuthal velocity. A further step not followed here is the conduction of a stability analysis to find the operating window where the predicted results are physically realizable (e.g. Huen, Frigaard & Martinez 2007; Lac & Sherwood 2009).

Velocity and pressure fields, as well as the shape of the liquid–liquid interface, are defined by the governing equations that impose conservation of mass and momentum for a non-inertial incompressible fluid, subjected to the appropriate boundary conditions. The subscript $k = 1, 2$ labels the two liquids considered. The conservation of mass is given by

$$\frac{1}{r}\frac{\partial}{\partial r}(r v_k) + \frac{\partial u_k}{\partial x} = 0, \tag{2.1}$$

while the equations for conservation of momentum are given by

$$\frac{1}{r}\frac{\partial}{\partial r}\left(r T_{(xr)_k}\right) + \frac{\partial}{\partial x}\left(T_{(xx)_k}\right) = 0, \tag{2.2}$$

$$\frac{1}{r}\frac{\partial}{\partial r}\left(r T_{(rr)_k}\right) - \frac{T_{(\theta\theta)_k}}{r} + \frac{\partial}{\partial x}\left(T_{(rx)_k}\right) = 0, \tag{2.3}$$

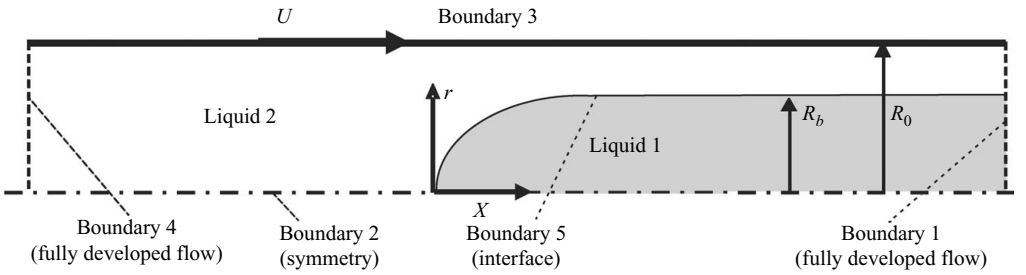

FIGURE 3. Boundary conditions considered for the problem.

where u and v are, respectively, the axial and radial components of the velocity field $\boldsymbol{u}$ and the quantities T_{xx}, T_{xr}, T_{rx}, T_{rr} and $T_{\theta\theta}$ are the components of the stress tensor $\boldsymbol{T}$.

For the description of the boundary conditions, boundaries are labelled from 1 to 5, as illustrated in figure 3. In the upstream far from the interface, Boundary 4, the flow is taken to be fully developed and the pressure is assumed to be uniform. Hence,

$$\boldsymbol{n}\cdot\nabla\boldsymbol{u}_2 = 0, \qquad p_2 = P_{in}, \tag{2.4}$$

where $\boldsymbol{n}$ is the unit vector normal to the boundary surface and p_2 is the constant pressure field on Phase 2 at the inlet.

Downstream, far from the cap of the drop, Boundary 1, the flow is also assumed to be fully developed, but the pressure is not imposed, which leads to

$$\boldsymbol{n}\cdot\nabla\boldsymbol{u}_k = 0. \tag{2.5}$$

Along the symmetry axis, Boundary 2, both the shear stress and the radial velocity vanish. Hence,

$$\boldsymbol{n}\cdot[\boldsymbol{T}_k\cdot\boldsymbol{t}] = 0, \qquad \boldsymbol{n}\cdot\boldsymbol{u}_k = 0, \tag{2.6}$$

where $\boldsymbol{t}$ is a unit vector tangent to the boundary surface.

No-slip and impermeability conditions are imposed along the tube wall, Boundary 3. Therefore,

$$\boldsymbol{u}_2 = U\boldsymbol{e}_x, \tag{2.7}$$

where $\boldsymbol{e}_x$ is the unit vector in the x-direction.

At the liquid–liquid interface, Boundary 5, the traction balances the capillary pressure, and there is no mass flow across the interface. Equation (2.8) is implemented adding the capillary pressure at every point of the interface. In this sense, the interface can be considered as part of Liquid 2. These conditions can be translated by

$$\boldsymbol{n}(p_1 - p_2) + \boldsymbol{n}\cdot(\boldsymbol{\tau}_2 - \boldsymbol{\tau}_1) = \frac{\sigma}{R_m}\boldsymbol{n}, \tag{2.8}$$

where $\boldsymbol{\tau}_k$ is the extra-stress tensor ($\boldsymbol{\tau}_k = \boldsymbol{T}_k + p_k\mathbf{I}$, where $\mathbf{I}$ is the identity tensor) and

$$\boldsymbol{u}_1 = \boldsymbol{u}_2 = (\boldsymbol{u}_k\cdot\boldsymbol{t})\,\boldsymbol{t}. \tag{2.9}$$

So the velocity component normal to the interface vanishes. In (2.8), σ is the liquid–liquid interfacial tension and p_1 and p_2 are the pressures on Phase 1 and Phase 2, respectively; $1/R_m$ is the local mean curvature of the interface, defined as

$$\frac{1}{R_m} \equiv \nabla_H\cdot\boldsymbol{n} \equiv \nabla\cdot\boldsymbol{n} - (\boldsymbol{n}\boldsymbol{n}\cdot\nabla)\cdot\boldsymbol{n}, \tag{2.10}$$

where the operator $\nabla_H \cdot ()$ is the divergence operator resolved in the tangential plane. For the axisymmetric case, the mean curvature vector can be written as

$$\frac{1}{R_m}\boldsymbol{n} = \frac{1}{\sqrt{x_s^2 + r_s^2}}\frac{\partial \boldsymbol{t}}{\partial s} - \frac{x_s}{r\sqrt{x_s^2 + r_s^2}}\boldsymbol{n}, \tag{2.11}$$

where s is the arclength curvilinear co-ordinate along the interface in the r–x plane and x_s and r_s are spatial derivatives with respect to s.

In (2.8), σ/R_m is the normal stress jump due to the interfacial tension, while the tangential stress at the interface is continuous.

The dimensionless parameters relevant to this kind of flow are the capillary number (Ca) and the viscosity ratio (N_μ), presented previously.

3. Theoretical analysis

The objective of the theoretical analysis is to extract every possible information from each of the fully developed regions and the relations between them. As will become clear, we were able to (a) provide alternative methods for the calculation of the residual mass fraction, (b) verify that $N_\mu = 2$ divides the problem into two branches and that when $N_\mu \leqslant 2$ the flow cannot have a bypass regime (independent of the value of Ca), (c) establish the relation between the critical mass fraction (defined and explained in § 3.3) and the viscosity ratio and (d) interpret and propose new dimensionless numbers that better characterize the flow regimes of sizes $\mathrm{L_I}$, $\mathrm{L_{II}}$, $\mathrm{L_{III}}$, and $\mathrm{L_{IV}}$.

Figure 1 shows the physical domain divided into four regions (length of regions defined by L). Region I and Region IV are regions in which the flow is fully developed and, therefore, streamlines are parallel to the wall. The axial co-ordinate of the tip of the drop marks the limit between Region II and Region III. Region II, occupied by Liquid 2 only, begins where the velocity profile departs from the fully developed one. The end limit of Region III is the point at which the velocity achieves its new fully developed profile.

3.1. *Global conservation of mass*

The velocity profile of Liquid 2 in Region I, $u_2^I(r)$, can be calculated using the boundary conditions $u_2^I(R_0) = U$ and finite shear stress at the centreline. The flow rate Q_2^I is given by

$$Q_2^I = U\pi R_0^2\left[1 - \frac{R_0^2}{8\mu_2 U}\left.\frac{\mathrm{d}p}{\mathrm{d}x}\right|_I\right] = U\pi R_0^2\left[1 - \left.\frac{\mathrm{d}p}{\mathrm{d}x}\right|_I^*\right], \tag{3.1}$$

where $(\mathrm{d}p/\mathrm{d}x)^*$ is a dimensionless pressure drop, constructed from the characteristic stress in Liquid 2, as follows:

$$\left.\frac{\mathrm{d}p}{\mathrm{d}x}\right|^* = \frac{\frac{1}{8}\frac{\mathrm{d}p}{\mathrm{d}x}R_0}{\frac{\mu_2 U}{R_0}}. \tag{3.2}$$

The velocity profiles of Liquid 1 and Liquid 2 at the fully developed Region IV can be calculated using the symmetry condition at the centreline, the known velocity at the wall and the compatibility conditions of continuity of velocity and the tangential stress at the interface.

The flow rates Q_2^{IV} and Q_1^{IV} are, thus, given by

$$Q_2^{IV} = U\pi R_0^2 \left[m - \left.\frac{\mathrm{d}p}{\mathrm{d}x}\right|_{IV}^{*} m^2 \right] \tag{3.3}$$

and

$$Q_1^{IV} = U\pi R_b^2 \left\{ 1 - \left.\frac{\mathrm{d}p}{\mathrm{d}x}\right|_{IV}^{*} [N_\mu (1-m) + 2m] \right\}, \tag{3.4}$$

where (1.1) and (3.2) have been used. It is worth noting that the pressure gradient in Region IV is the same for the two liquids, since by Young–Laplace, $p_1^{IV} - p_2^{IV} = \sigma/R_b$.

The global conservation of mass of Liquids 1 and 2 requires that

$$Q_2^{I} = Q_2^{IV} \tag{3.5}$$

$$Q_1^{IV} = 0. \tag{3.6}$$

From (3.4) and (3.6) we can find a relation between the dimensionless pressure gradient in Region IV and the mass deposited at the wall for a given viscosity ratio, which is given by

$$\left.\frac{\mathrm{d}p}{\mathrm{d}x}\right|_{IV}^{*} = \frac{1}{(2-N_\mu)m + N_\mu}. \tag{3.7}$$

Solving for m we find that

$$m = \frac{1 - N_\mu \left.\dfrac{\mathrm{d}p}{\mathrm{d}x}\right|_{IV}^{*}}{(2-N_\mu) \left.\dfrac{\mathrm{d}p}{\mathrm{d}x}\right|_{IV}^{*}}. \tag{3.8}$$

From (3.7) we can observe that $\mathrm{d}p*/\mathrm{d}x_{IV}$ is independent of m in two cases: when $N_\mu \to \infty$ (gas–liquid displacement) and when $N_\mu = 2$. The corresponding values for the dimensionless pressure gradient in Region IV are $\mathrm{d}p*/\mathrm{d}x_{IV} = 0$ and $\mathrm{d}p*/\mathrm{d}x_{IV} = 1/2$, respectively. Therefore, these cases leave m undetermined, not singular.

From (3.1), (3.3) and (3.5) we obtain a relation between the dimensionless pressure gradients in Region I and in Region IV. Using (3.7) we get an analogue of this equation for $\mathrm{d}p*/\mathrm{d}x_I$:

$$\left.\frac{\mathrm{d}p}{\mathrm{d}x}\right|_{I}^{*} = m^2 \left.\frac{\mathrm{d}p}{\mathrm{d}x}\right|_{IV}^{*} + 1 - m = \frac{m^2}{(2-N_\mu)m + N_\mu} + 1 - m. \tag{3.9}$$

Solving the first equation for m we have that

$$m_-^+ = \frac{1}{2\left.\dfrac{\mathrm{d}p}{\mathrm{d}x}\right|_{IV}^{*}} \pm \sqrt{\left(\frac{1}{2\left.\dfrac{\mathrm{d}p}{\mathrm{d}x}\right|_{IV}^{*}}\right)^2 - \frac{1 - \left.\dfrac{\mathrm{d}p}{\mathrm{d}x}\right|_{I}^{*}}{\left.\dfrac{\mathrm{d}p}{\mathrm{d}x}\right|_{IV}^{*}}}. \tag{3.10}$$

From (3.9) we verify that $m(\mathrm{d}p*/\mathrm{d}x_{IV} = 0) = 1 - \mathrm{d}p*/\mathrm{d}x_I$. Hence, in the gas–liquid displacement problem, the dimensionless pressure gradient in Region I is the fraction of mass 'not attached' to the wall, giving to $\mathrm{d}p*/\mathrm{d}x_I$ another interpretation in this case.

An important aspect of the analysis is that we are considering a two-layer flow in Region IV and, therefore, the restriction

$$0 < m < 1. \tag{3.11}$$

The two inequalities given by relation (3.11) can be combined with (3.8) and (3.10) to impose restrictions on $\mathrm{d}p*/\mathrm{d}x_I$ and $\mathrm{d}p*/\mathrm{d}x_{IV}$. These restrictions lead to the following conclusions:

$$N_\mu > 2 \Rightarrow \frac{1}{N_\mu} < \left.\frac{\mathrm{d}p}{\mathrm{d}x}\right|_{IV}^{*} < \frac{1}{2} \text{ and } \left.\frac{\mathrm{d}p}{\mathrm{d}x}\right|_{IV}^{*} < 1 - \frac{1}{4\left.\dfrac{\mathrm{d}p}{\mathrm{d}x}\right|_{IV}^{*}} < \left.\frac{\mathrm{d}p}{\mathrm{d}x}\right|_{I}^{*} < 1. \tag{3.12}$$

$$N_\mu < 2 \Rightarrow \frac{1}{2} < \left.\frac{\mathrm{d}p}{\mathrm{d}x}\right|_{IV}^{*} < \frac{1}{N_\mu} \text{ and } 1 - \frac{1}{4\left.\dfrac{\mathrm{d}p}{\mathrm{d}x}\right|_{IV}^{*}} < \frac{1}{2} < \left.\frac{\mathrm{d}p}{\mathrm{d}x}\right|_{I}^{*}. \tag{3.13}$$

$$N_\mu = 2 \Rightarrow 1 - \frac{1}{4\left.\dfrac{\mathrm{d}p}{\mathrm{d}x}\right|_{IV}^{*}} = \left.\frac{\mathrm{d}p}{\mathrm{d}x}\right|_{IV}^{*} = \frac{1}{2} < \left.\frac{\mathrm{d}p}{\mathrm{d}x}\right|_{I}^{*} < 1. \tag{3.14}$$

The results given by inequalitites (3.12)–(3.14) show the non-intuitive result that when a fluid is displacing another one which has a viscosity twice that of the displacing fluid, it is a special case that splits the problem into two branches. Interestingly, Lac & Sherwood (2009), using boundary integral computations to investigate the pressure-driven flow of a finite drop in a capillary tube, also found a two-branched behaviour with $N_\mu = 2$ as a boundary between the cases. Inequality (3.11) also avoids complex values for m when solving (3.10).

When the two viscosities are equal, the dependence of (3.9) on m^2 is eliminated. The compatibility between this case and inequality (3.11) can only be justified by $Ca < \infty$, since the conditions $N_\mu = 1$ and $Ca = \infty$ would mean the two fluids are the same. For the case $N_\mu = 1$ and $Ca < \infty$ the dimensionless pressure gradients in Regions I and IV are equal.

Equations (3.9) and (3.8) can be combined to calculate $\mathrm{d}p*/\mathrm{d}x_I$ as a function of $\mathrm{d}p*/\mathrm{d}x_{IV}$ and N_μ. The result is

$$\left.\frac{\mathrm{d}p}{\mathrm{d}x}\right|_{I}^{*} = \frac{(N_\mu - 1)\left(1 - 4\left.\dfrac{\mathrm{d}p}{\mathrm{d}x}\right|_{IV}^{*}\right) + N_\mu^2 \left.\dfrac{\mathrm{d}p}{\mathrm{d}x}\right|_{IV}^{*2}}{(N_\mu - 2)^2 \left.\dfrac{\mathrm{d}p}{\mathrm{d}x}\right|_{IV}^{*}}. \tag{3.15}$$

For the reasons previously discussed, $\mathrm{d}p*/\mathrm{d}x_I$ is not unbounded for $N_\mu = 2$ and nor is $\mathrm{d}p*/\mathrm{d}x_{IV} = 0$.

3.2. *Force balance at the interface in Region IV*

Since the tangential force is continuous through the interface, when this condition is applied to the interface in Region IV, we find that

$$N_\mu = \frac{\mu_2}{\mu_1} = \left.\frac{\dfrac{\partial u_1^{IV}}{\partial r}}{\dfrac{\partial u_2^{IV}}{\partial r}}\right|_{r=R_b} = \left.\frac{\dfrac{\partial u_1^{IV*}}{\partial r^*}}{\dfrac{\partial u_2^{IV*}}{\partial r^*}}\right|_{r^*=\frac{R_b}{R_0}}. \tag{3.16}$$

This result shows that the viscosity ratio is related to the velocity gradient jump at the interface.

A dimensionless form of the Young–Laplace equation can be constructed to represent how forces normal to the interface in Region IV equilibrate. We chose

to compare the pressure drop from the centreline to a point just after the interface, with the pressure drop that represents a head loss of the flow, $\mathrm{d}p/\mathrm{d}x_I$. The result is

$$N_\sigma = \frac{\dfrac{p_1^{IV} - p_2^{IV}}{R_b}}{\dfrac{1}{8}\left.\dfrac{\mathrm{d}p}{\mathrm{d}x}\right|_I} = \frac{\sigma R_0^2}{\mu_2 U R_b^2 \left.\dfrac{\mathrm{d}p}{\mathrm{d}x}\right|_I^*} = \frac{1}{Ca(1-m)\left.\dfrac{\mathrm{d}p}{\mathrm{d}x}\right|_I^*}. \tag{3.17}$$

Another dimensionless number that can be useful to explain the behaviour of the flow is one that represents the competition between the tangential and normal forces at the interface between the two fluids in Region IV, such as N_μ/N_σ.

3.3. *Critical condition*

Before we proceed further with our analysis we must define the notion of a 'transition window'. In the present case, it corresponds to a two-dimensional region in the space formed by the parameters Ca and N_μ, within which the flow is neither in the bypass regime nor in the full-recirculation one. Bypass flow patterns are characterized by the absence of recirculation on the fluid which is being displaced. The full-recirculation regime is characterized not only by the presence of recirculation in the displaced liquid but also by the presence of a secondary recirculation in the displacing liquid. A critical case can be achieved when the flow regime is located at the boundary of the transition window, i.e. when the flow starts the departure from the bypass regime towards the full-recirculation one, in a trajectory in the $Ca \times N_\mu$ space. The conditions for this critical case are accomplished when the centreline velocity of Liquid 2 in Region I vanishes; that happens when $\mathrm{d}p^*/\mathrm{d}x_I = 1/2$. If we substitute this result in (3.9), we find a quadratic equation with $m_c = 1$ as one of the solutions. Since we are searching for solutions that satisfy inequality (3.11), the only possible physical solution is

$$m_c = \frac{1}{2\left(1 - \dfrac{1}{N_\mu}\right)}. \tag{3.18}$$

The result given by (3.18) is the generalization, concerning liquid–liquid displacement, of the result given by Taylor (1961) for the gas–liquid displacement, where $m_c = 0.5$. When $N_\mu \to \infty$, Taylor's result is obtained. Now, if we combine (3.18) with inequality (3.11) we find that $N_\mu > 2$ is a restriction on the viscosity ratio for the existence of a critical value for m. This result shows that for $N_\mu \leqslant 2$ the flow can never achieve the boundary of the transition region, and therefore, it will not develop the two different limiting regimes. By examining relations (3.13) and (3.14), we can see that $\mathrm{d}p^*/\mathrm{d}x_I > 1/2$ in this case, and therefore, the bypass flow pattern is the regime not achieved when $N_\mu \leqslant 2$.

The derivative of m_c with respect to N_μ is strictly negative, which shows that the critical value for the fraction of mass increases when N_μ decreases.

4. Numerical implementation

4.1. *Elliptic grid generation*

Due to the position of the interface, the flow domain, for each fluid, is unknown *a priori*. In order to tackle this problem by means of standard techniques for boundary value problems, the approach used in the present work is to transform the set of differential equations and boundary conditions written for the physical domain into an

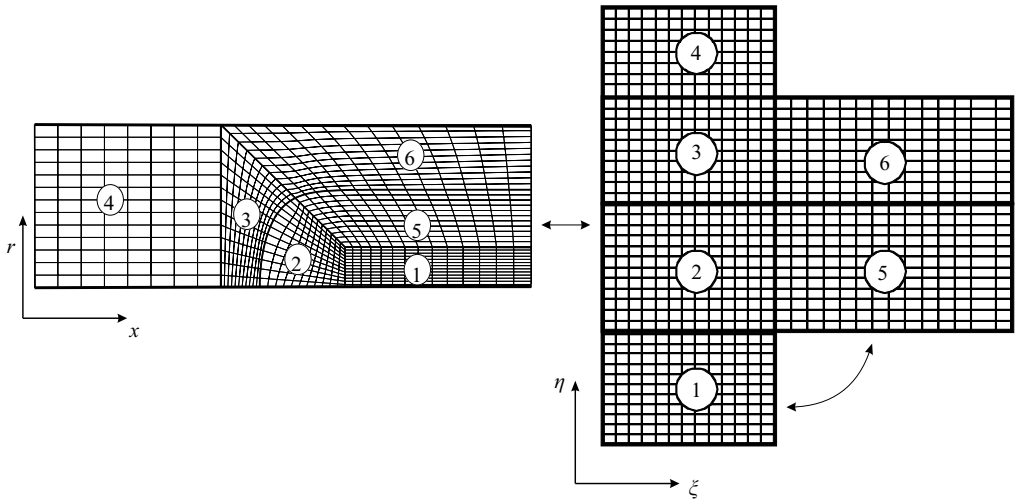

FIGURE 4. Mapping between the physical and the reference domain.

equivalent set, defined in a known reference domain. For a complete understanding of the method employed the reader is referred to the works of Christodoulou & Scriven (1992), Sackinger, Shunk & Rao (1996) and Dimakopoulos & Tsamopoulos (2003*a*). This transformation is achieved by a mapping function $\boldsymbol{x} = \boldsymbol{x}(\xi)$ that connects the two domains, as shown in figure 4. A functional of weighted smoothness can be used successfully to construct the type of mapping involved here. The inverse of the mapping that minimizes the functional is governed by a pair of elliptic differential equations that are identical to those encountered in diffusional transport phenomena with variable diffusion coefficients. The co-ordinates ξ and η of the reference domain must satisfy

$$\nabla \cdot (D_\xi \nabla \xi) = 0, \tag{4.1}$$

$$\nabla \cdot (D_\eta \nabla \eta) = 0, \tag{4.2}$$

where D_ξ and D_η are diffusion-like coefficients used to control gradients in co-ordinate potentials and, thereby, the spacing between the curves of constant ξ on one hand and of constant η on the other that make up the sides of the quadrilateral elements that were employed. Equations (4.1) and (4.2) describe the inverse mapping $\boldsymbol{\xi} = \boldsymbol{\xi}(\boldsymbol{x})$. To evaluate $\boldsymbol{x} = \boldsymbol{x}(\boldsymbol{\xi})$, the diffusion equations that describe the mapping also have to be transformed to the reference configuration.

Following the ideas introduced in Christodoulou & Scriven (1992), Dimakopoulos & Tsamopoulos (2003*a*,*b*, 2004, 2007) have used different functions for the coefficients D_ξ and D_η for the transient gas displacement of Newtonian, viscoplastic and viscoelastic materials, depending on the direction of the advancing front. The coefficients that gave the best results were $D_\eta = 1$ and

$$D_\xi = \epsilon \sqrt{\frac{r_\xi^2 + z_\xi^2}{r_\eta^2 + z_\eta^2}} + 1 - \epsilon, \tag{4.3}$$

where ϵ is a weighting parameter adjusted by trial and error to optimize the performance of the mesh generation scheme; usually it is set to 0.1 ($\epsilon = 0$ corresponds to $D_\xi = 1$).

In the present work we adopt a different approach which is more suitable for steady-state problems. This approach has already been adopted by Soares *et al.* (2005), but the novelty introduced was not explained. Hence, for a better understanding, we briefly describe below the main difference between this approach and the one presented by Dimakopoulos & Tsamopoulos (2003*a*).

We divide the reference and physical domains into quadrilateral sub-domains. Therefore, the distribution generated on the boundaries of a sub-domain is diffused to the interior of it. By doing this, we can relax the complexity of the diffusion coefficients and keep them as $D_\xi = D_\eta = 1$. Depending on the problem a different number of sub-domains is necessary. In the case of the present work we adopt six sub-domains (see figure 4). Sub-domains 1 and 4 are far from the interface; hence, the present arrangement enables freezing the nodal points inside these sub-domains. In other words, differently from what happened in Soares *et al.* (2005), (4.1) and (4.2) do not need to be solved in sub-domains 1 and 4, saving computational costs. Another peculiarity of the problem is the impossibility to split the physical domain occupied by Liquid 1 into quadrilateral sub-domains with the same orientation. In other words if we label the boundaries of a sub-domain with north, south, east and west, a north/south boundary is seen, from the perspective of a neighbourhood sub-domain, as an east/west boundary. In particular, the boundary between sub-domains 1 and 5 is a constant ξ-line looking from the perspective of sub-domain 1 and is a constant η-line looking from the perspective of sub-domain 5. In figure 4, the west side of sub-domain 1 and the south side of sub-domain 5 correspond to a unique set of points.

The gradient of the mapping $\boldsymbol{x} = \boldsymbol{x}(\xi)$ in a two-dimensional domain is defined as $\mathbf{J} \equiv \nabla_\xi \boldsymbol{x}$. The Jacobian of the transformation is $\|\mathbf{J}\| = \det\mathbf{J}$. Boundary conditions are needed in order to solve the second-order partial differential equations $\boldsymbol{\xi} = \boldsymbol{\xi}(\boldsymbol{x})$. Spatial derivatives with respect to the co-ordinates of the physical domain $\boldsymbol{x}$ can be written in terms of the derivatives with respect to the co-ordinates of the reference domain $\boldsymbol{\xi}$ by using the inverse of the mapping gradient, that is

$$\begin{pmatrix} \dfrac{\partial}{\partial x} \\ \dfrac{\partial}{\partial r} \end{pmatrix} = \mathbf{J}^{-1} \begin{pmatrix} \dfrac{\partial}{\partial \xi} \\ \dfrac{\partial}{\partial \eta} \end{pmatrix}. \tag{4.4}$$

Along the solid walls, symmetry planes and synthetic inlet and outlet planes, the boundary is located by imposing a relation between co-ordinates x and r, and stretching functions are used to distribute the nodal points of the finite-element mesh along the boundaries. The same procedure is applied for the non-interface boundaries between sub-domains. The points located at the boundaries between sub-domains 2 and 5 and between sub-domains 3 and 6 belong to the same linear function between x and r. For sub-domains 1, 5 and 6, an exponential function was used to concentrate points close to the front of the drop. For the other boundaries the distribution was uniform. The position of the liquid–liquid interface is located by imposing the condition stated by (2.9) on the boundaries between sub-domains 5 and 6 and between sub-domains 2 and 3.

Two representative meshes for the same pair (Ca, N_μ) are shown in figure 5. The difference between them is the given inlet pressure. Since sub-domains 1 and 4 are of fixed sizes, sub-domains 2 and 3 change their refinement according to this boundary condition. It can be shown that when pressure gradient is greater in Region I than in

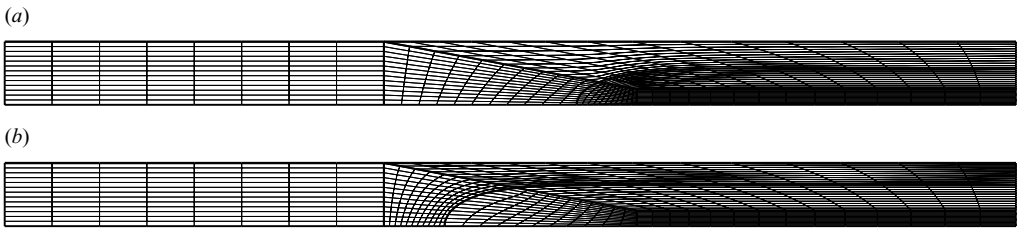

FIGURE 5. Typical meshes used (*a*) to capture the secondary recirculation in Phase 1 and (*b*) to capture the transition from the bypass and recirculation flow regimes.

Region IV, lower values of the inlet pressure would lead to meshes such as the one represented by figure 5(*a*), while higher values of P_{in}^{*} would lead to meshes as the one shown in figure 5(*b*).

4.2. *Solution of the equation system by Galerkin finite-element method*

The differential equations that govern the problem and the mapping (mesh generation) equations were solved all together by the Galerkin finite-element method as explained in Sousa *et al.* (2007). Biquadratic basis functions were used to represent the velocity and nodal co-ordinates, while linear discontinuous functions were employed to expand the pressure field. The coefficients of the expansions are the unknowns of the problem. The corresponding weighted residuals of the Galerkin method related to conservation of mass, to conservation of momentum and to mesh generation can be found in Soares *et al.* (2005).

4.3. *Solution of the nonlinear system of algebraic equation by Newton's method*

The set of simultaneous algebraic equations for the coefficients of the basis functions of all the fields is nonlinear and sparse. It was solved by Newton's method. In order to improve the initial guess it was necessary to solve intermediate problems. The first successful preliminary problem was computed using a fixed mesh with slippery surface (a surface that allows perfect slip) in place of the liquid–liquid interface as the initial condition for Newton's method.

The linear system of equations for each Newton iteration was solved using a frontal solver. A mesh convergence analysis was performed by increasing the number of elements until the solution changed by less that 1 %, and a set of mesh arrangements was analysed until the recirculation on the tip of the liquid–liquid interface had been captured precisely. In the final mesh architecture, as exemplified by figure 5, the domain is divided into 880 elements that correspond to 3635 nodes and 17 180 degrees of freedom.

5. Results and discussion

Since we are concerned with the flow patterns the problem exhibits, and the three kinds of flow regimes are only possible for $N_\mu > 2$, the numerical analysis is restricted to $N_\mu \geqslant 2$, letting $N_\mu = 2$ be a limiting one.

Values of the viscosity ratio, chosen as to form a spectrum of possibilities, in order to analyse the effect of Ca on the problem being considered, were $N_\mu = 2,\ 4,\ 8$ and 400.

5.1. *Fraction of mass m*

The results for the residual mass fraction as a function of the capillary number for these viscosity ratios (figure 6) were used to test the accuracy of the numerical

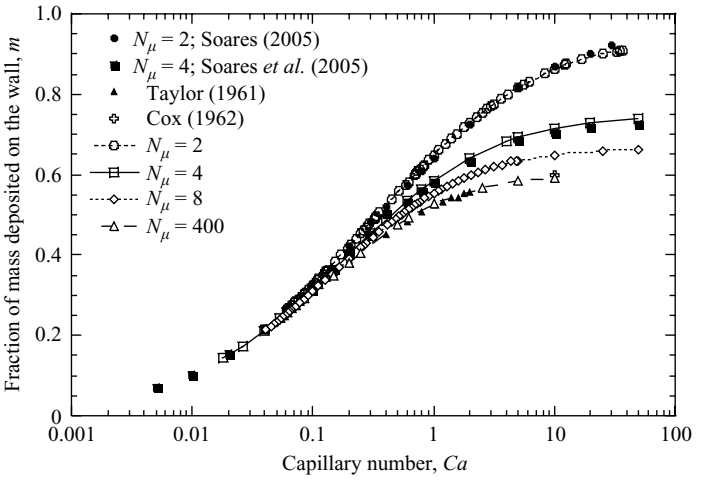

FIGURE 6. Fraction of deposited mass on the wall as a function of capillary number for a range of viscosity ratio and comparison with the previous prediction from Soares *et al.* (2005) and data from Taylor (1961) and Cox (1962).

method/scheme employed. For $N_\mu = 400$, the liquid–liquid displacement problem tends to the gas–liquid displacement. Therefore, the experimental results obtained by Taylor (1961) and Cox (1962) can be compared to the present ones. From figure 6, we can see that the numerical results of the present work (white triangles) follow the same curve as the experimental results (black triangles and cross). The relative difference in value was less than 1 % for a number of tested cases in which an interpolation of third order was used for experimental values between numerical results. Soares *et al.* (2005) made a comparison of the residual fraction of mass with some results of Goldsmith & Mason (1963) and found a relative difference of less than 1 %. In the present work a more refined mesh was used and the residual mass fraction was coincident with that of Soares *et al.* (2005) (less than 0.5 % in most of the cases). Therefore, we can infer that the errors, related to the experimental results of Goldsmith & Mason (1963) are of the same order of magnitude.

5.2. *Alternative methods for the determination of the residual mass fraction*

Using the continuity equation, it can be shown that the fraction of mass attached to the wall is also given by

$$m \equiv 1 - \frac{R_b^2}{R_0^2} = \frac{\bar{u}_2^I}{\bar{u}_2^{IV}}, \tag{5.1}$$

where $\bar{u}_2^I$ and $\bar{u}_2^{IV}$ are the mean velocities of Liquid 2 in Region I and in Region IV, respectively. For the gas-displacement case, $\bar{u}_2^{IV} \approx U$, and the residual mass fraction can be determined by the velocity of the propagating front and by measuring the rate at which the mass of the displaced fluid is leaving the tube. However, this procedure cannot be used for the liquid–liquid displacement, since $\bar{u}_2^{IV}$ is not measured. In this case, optical devices that can locate the value of R_b should be preferred. However, for non-transparent displaced fluids, such as dark oils, optical devices are not able to detect the inner fluid. Another possible detection problem could happen when it is difficult to distinguish one phase from another due to a similarity between the refractive indexes of the fluids. Equations (3.8) and (3.10) suggest alternative experimental methods for computing the fraction of mass deposited at the wall. Two

$N_\mu = 8$	A	B	m_n	m_1	E_1	m_2	E_2
$Ca = 50$	0.4465	0.2479	0.662	0.6611	0.14 %	0.6622	0.03 %
$Ca = 1$	0.5114	0.2126	0.554	0.5491	0.88 %	0.5538	0.03 %
$Ca = 0.1$	0.7047	0.1627	0.311	0.3087	0.74 %	0.3107	0.10 %

TABLE 1. Comparison between different ways to obtain the fraction of mass deposited on the wall for $N_\mu = 8$, where $A = \mathrm{d}p*/\mathrm{d}x_I$; $B = \mathrm{d}p*/\mathrm{d}x_{IV}$; $m_n = 1 - (R_b/R_0)^2$; $m_1 = (1 - N_\mu B)/(2 - N_\mu)B$; $m_2 = (1/2B) - \sqrt{(1/2B)^2 - (1 - A)/B}$.

$N_\mu = 4$	A	B	m_n	m_1	E_1	m_2	E_2
$Ca = 50$	0.4770	0.3913	0.739	0.7381	0.12 %	0.7337	0.72 %
$Ca = 1$	0.5357	0.3554	0.585	0.5929	1.35 %	0.5866	0.27 %
$Ca = 0.1$	0.7135	0.2964	0.316	0.3131	0.92 %	0.3161	0.03 %

TABLE 2. Comparison between some different form to obtain the fraction of mass deposited on the wall for $N_\mu = 4$, where $A = \mathrm{d}p*/\mathrm{d}x_I$; $B = \mathrm{d}p*/\mathrm{d}x_{IV}$; $m_n = 1 - (R_b/R_0)^2$; $m_1 = (1 - N_\mu B)/(2 - N_\mu)B$; $m_2 = (1/2B) - \sqrt{(1/2B)^2 - (1 - A)/B}$.

nearby pressure transducers attached to the tube wall can be used to measure the pressure drop in Regions I and IV and the velocity of the interface, as explained next. These transducers would provide two curves of pressure as a function of time. When the front of the drop is far from the transducers, pressure will drop linearly, and thus, $\mathrm{d}p/\mathrm{d}x_I$ and $\mathrm{d}p/\mathrm{d}x_{IV}$ can be calculated. A deviation from its linear behaviour would indicate that Regions II and III are passing through the transducers' longitudinal position. There will be a time delay, from one transducer to the other, for the detection of the nonlinear pressure behaviour. The distance between the transducers divided by this time delay would give a measure for the velocity of the propagating front. With these measurements, (3.8) and (3.10) provide two independent approximated values for m (one of the roots of (3.10) is always out of the range $]0, 1[$). In figure 6 the procedure to determine m was to infer, from the numerical results, the position of the interface. Tables 1 and 2 show results obtained from (3.8) and (3.10), m_1 and m_2, respectively, and how they compare with our numerical value obtained from the position of the interface, m_n, for the values of capillary number $Ca = 0.1$, 1.0 and 50. Table 1 refers to the results obtained for $N_\mu = 8$, while table 2 refers to the results obtained for $N_\mu = 4$. We chose different positions in Regions I and IV to measure the dimensionless pressure gradients $\mathrm{d}p*/\mathrm{d}x_I$ and $\mathrm{d}p*/\mathrm{d}x_{IV}$, and therefore, the values that fill the tables are average values. The percentage difference E_i is calculated as follows:

$$E_i = \frac{|m_i - m_n|}{m_n} \times 100. \tag{5.2}$$

These results show that the theoretical analysis that led to (3.8) and (3.10) is in agreement with our numerical calculation. This can be seen as another accuracy test of our numerical method/scheme, since three different ways of calculating the same quantity led to the same result (within a relative error of less than 1 %).

Equation (3.8) does not need the measurement of $\mathrm{d}p*/\mathrm{d}x_I$ as in (3.10). However, the same apparatus set-up provides the measurement of this quantity. Hence, the two equations are equivalent in giving indirect measures of m.

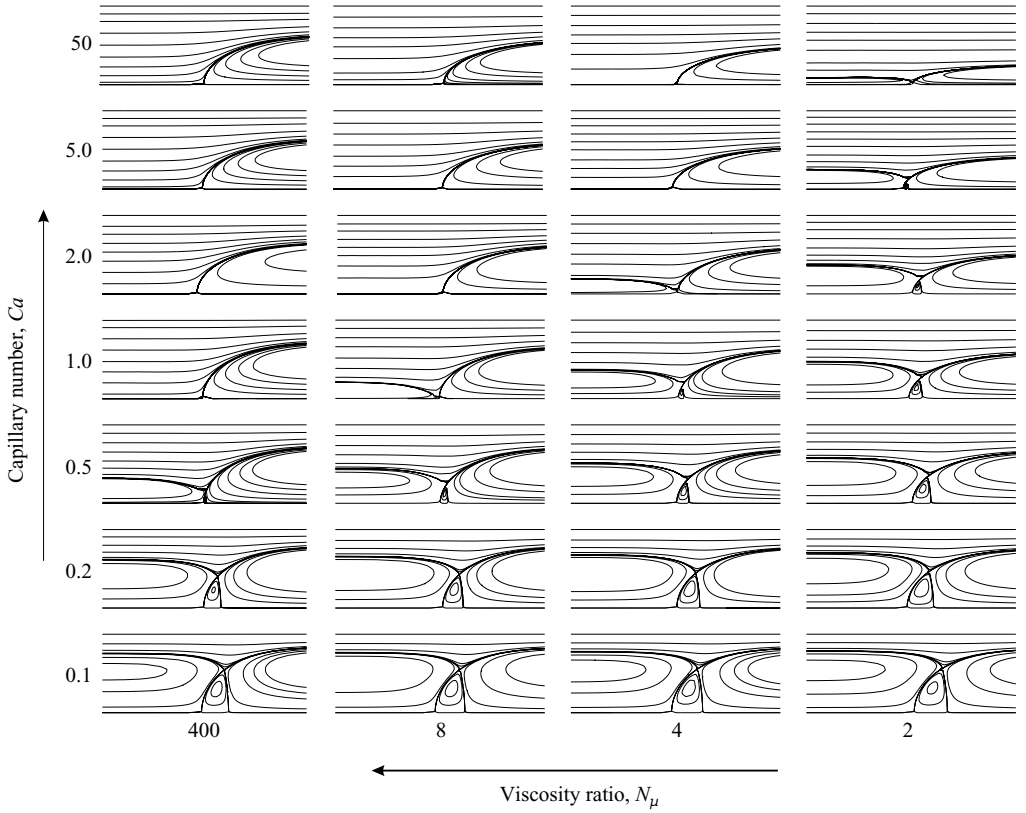

FIGURE 7. Streamline patterns near the liquid–liquid interface given in a Cartesian manner in a $Ca \times N_\mu$ space: transitions from bypass to recirculation flow regimes from the perspective of Phase 2.

5.3. *Streamline patterns*

Figure 7 depicts a set of examples of the streamlines in the neighbourhood of the tip of the interface between the two liquids, given in a Cartesian manner. These cases were built to cover qualitatively the main aspects of the space ($N_\mu \geqslant 2 \times Ca$). This figure shows the influence of the dimensionless parameters, the viscosity ratio and the capillary number, on the different flow patterns that this problem presents.

The spectrum of capillary numbers chosen to compose the complete frame were $Ca = 0.1$, 0.2, 0.5, 1.0, 2.0, 5.0 and 50. We can observe that for higher values of the capillary number and higher values of the viscosity ratio, we have bypass regimes. On the other side of this tendency, for lower values of Ca and N_μ, the cases are of full-recirculation flow in which a secondary recirculation appears within the displacing fluid domain near the finger tip. As discussed previously, $N_\mu = 2$ does not present the bypass flow regime in this case. We can also observe a limiting value Ca^L ($0.5 < Ca^L < 1$), below which there is no transition either, independently on the value of N_μ. This result was not predicted in the theoretical analysis. However, in general, we have that for a fixed viscosity ratio, there is a range of capillary numbers of transition between the two extreme flow patterns and that this range occurs for decreasing values of Ca as N_μ increases.

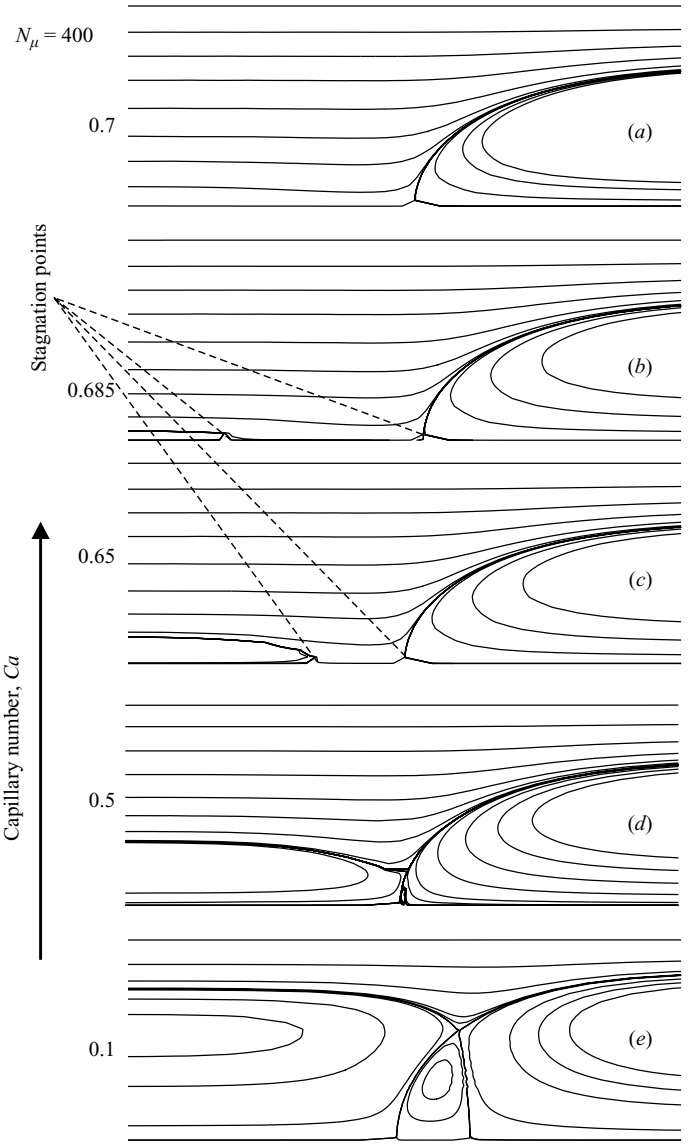

FIGURE 8. Streamline patterns in liquid–liquid displacement for fixed viscosity ratio, $N_\mu = 400$, and a fine range for the capillary number around its transition value from bypass to recirculation flow regimes.

Figures 8–10 show the two flow regimes and a refinement in the capillary number in the transition range for fixed viscosity ratios, $N_\mu = 400$, 8 and 4, respectively. We can notice that here are some kinks in the streamlines in these figures, and ideally, there would be room for a mesh refinement improvement. However, the convergence of these cases with the present number of degrees of freedom is extremely difficult. Besides freezing the nodal points in sub-domains 1 and 4, more intermediate cases were necessary to solve the problem with the current method and achieve the streamline accuracy shown in these figures, even though they are illustrative in the sense that they give a reasonably accurate location of the values of critical

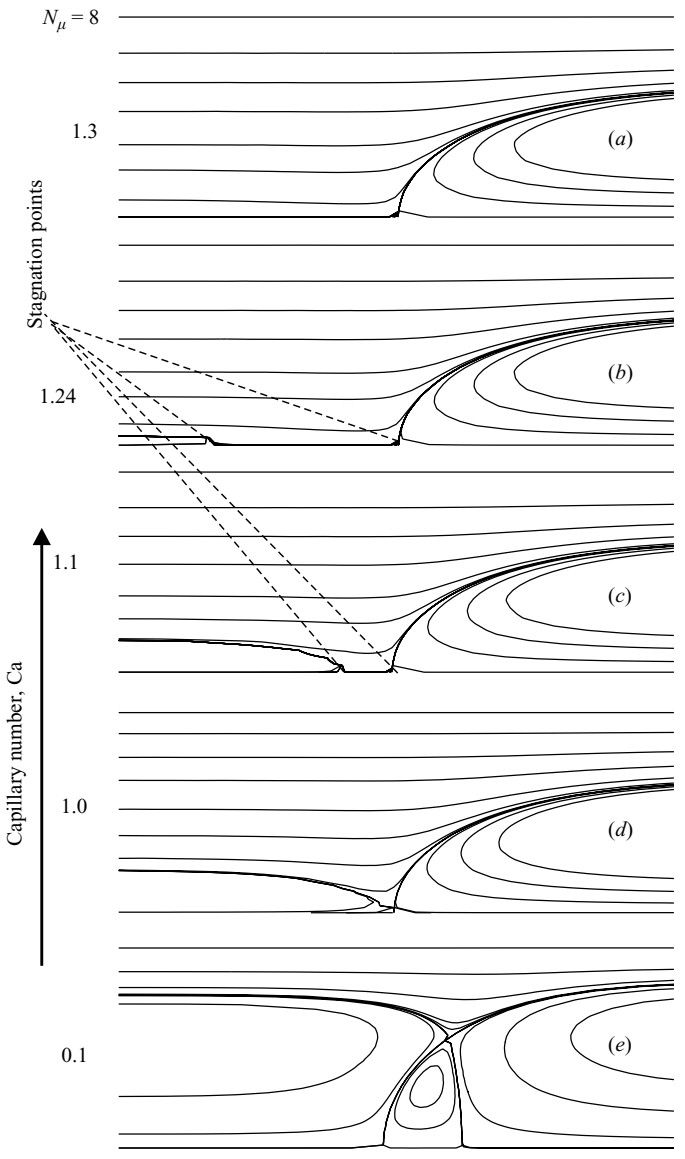

FIGURE 9. Streamline patterns in liquid–liquid displacement for fixed viscosity ratio, $N_\mu = 8$, and a fine range for the capillary number around its transition value from bypass to recirculation flow regimes.

Capillary number corresponding to the boundary of the transition window. We hope these results can be compared by future experimental and numerical investigation of the problem. Moreover, an important qualitative consequence of this analysis is that for the conditions analysed, the patterns formed during transition are similar to the ones obtained for the gas–liquid displacement of a Newtonian fluid, since there are no closed recirculations near the tip of the interface at the displaced fluid side, different from the ones sketched by Hodges *et al.* (2004), where the limit $Ca \to 0$ was considered, and numerically obtained by Sousa *et al.* (2007), where the gas-displacement of non-Newtonian fluids were considered.

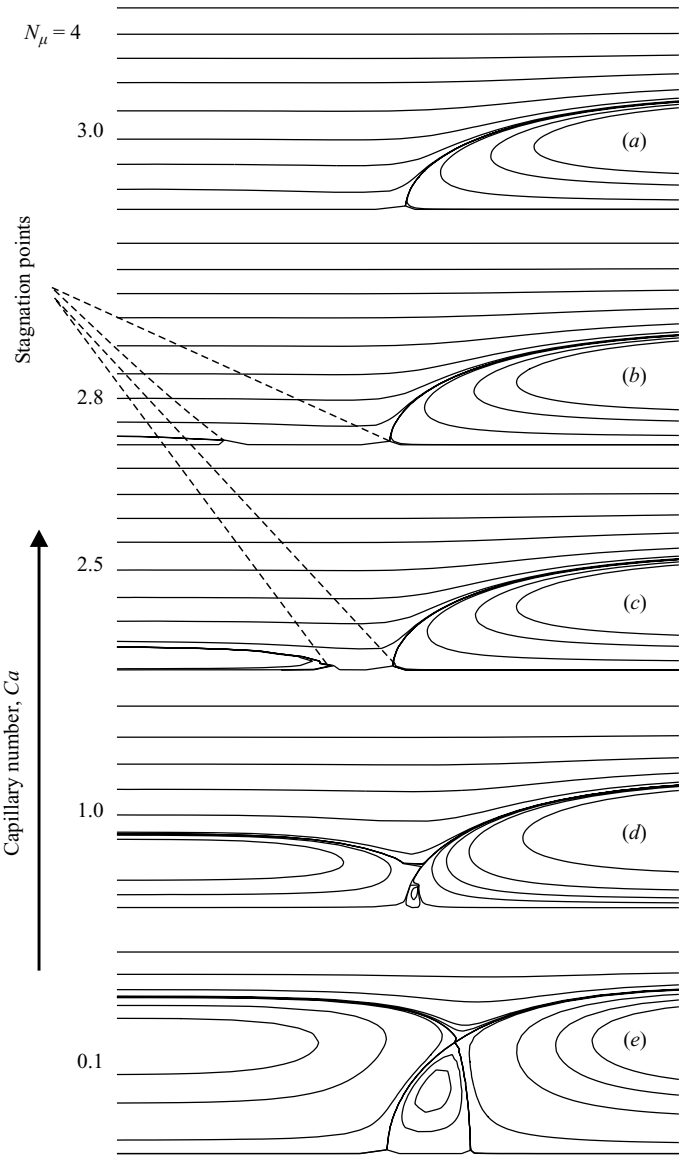

FIGURE 10. Streamline patterns in liquid–liquid displacement for fixed viscosity ratio, $N_\mu = 4$, and a fine range for the capillary number around its transition value from bypass to recirculation flow regimes.

For the case $N_\mu = 400$ (figure 8), we can see that the critical capillary number is $0.685 < Ca_c < 0.7$. This result is in accordance with the ones obtained by Sousa *et al.* (2007) for gas displacing a Newtonian liquid, where they found that $0.6 < Ca_c < 0.7$. For $N_\mu = 8$ and $N_\mu = 4$, the critical capillary number increases to $1.24 < Ca_c < 1.3$ and $2.8 < Ca_c < 3.0$, respectively. In order to give a precise value for this critical capillary number, we use the corresponding critical fraction of mass deposited at the wall, calculated from (3.18), namely $m_c(N_\mu = 4) = 2/3$, $m_c(N_\mu = 8) = 4/7$ and $m_c(N_\mu = 400) = 200/399$. The critical capillary numbers using an interpolation of third order of the numerical results were $Ca_c(N_\mu = 4) = 2.825$, $Ca_c(N_\mu = 8) = 1.273$

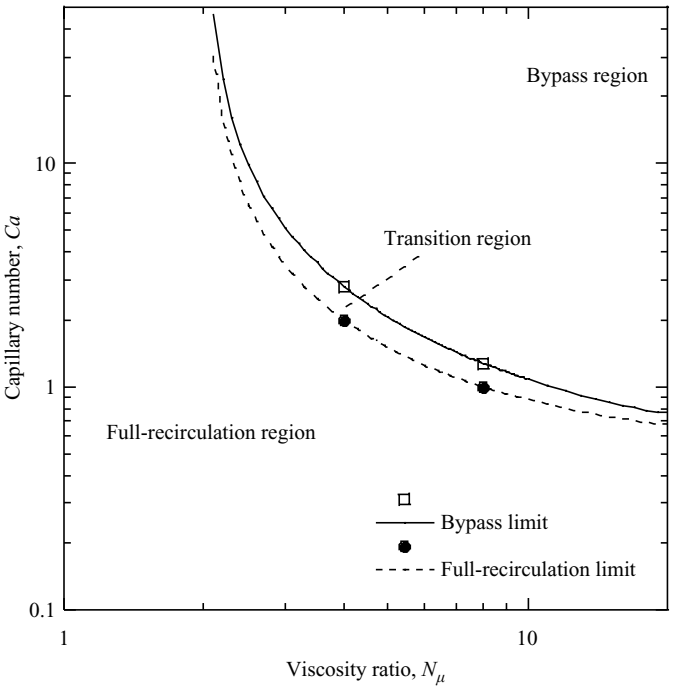

FIGURE 11. Qualitative curves limiting the transition region between bypass and full-recirculation flow patterns.

and $Ca_c(N_\mu = 400) = 0.696$, which are in agreement with the ranges indicated by figures 8–10.

Finally, in figure 11, we use an interpolation function to sketch two qualitative curves that limit the region of transition between bypass and full-recirculation flow regimes in the Cartesian space $Ca \times N_\mu$. The asymptote $N_\mu = 2$ was obtained theoretically. The values corresponding to $N_\mu = 4$ and $N_\mu = 8$ as well as the asymptotes corresponding to the $N_\mu \to \infty$ were obtained numerically. These point values and asymptotes are, thus, included in the interpolation function. This result gives an idea of which kind of flow regime is expected for a given pair (Ca, N_μ).

6. Final remarks

A theoretical and numerical analysis has been conducted on the problem of the liquid–liquid displacement of two immiscible viscous fluids in a capillary tube for the case in which a film of the displaced fluid remains attached to the wall as the displacing fluid moves.

The theoretical analysis has shown a non-intuitive result that was essential for the conduction of the numerical investigation, namely that the case in which the viscosity of the displaced fluid is twice the viscosity of the injected fluid splits the problem into two branches. The reason for that can be explained by the continuity equation, applied for the two liquids in the fully developed regions. For $N_\mu \leqslant 2$ the critical value for the dimensionless pressure gradient in Region I is never achieved and the flow regime cannot be a bypass flow. Hence, when $N_\mu > 2$, the flow considered can present the two extreme flow patterns considered by Taylor (1961), namely bypass and full-recirculation regimes, and the transition between them, where there are two

stagnation points. (In fact Taylor 1961 did not use the word transition and did not mention that parameterized by a quantity, Ca, the flow regime with two stagnation points was 'in between' the other cases.) The general expression for entering the bypass regime is

$$m_c = \frac{1}{2\left(1 - \dfrac{1}{N_\mu}\right)} \tag{6.1}$$

and is reduced to $m_c = 0.5$ (Taylor 1961), as a limit, when gas-displacement ($N_\mu \to \infty$) is considered.

We have also found alternative methods, without the need to measure the interface position visually, to calculate the fraction of mass attached to the wall by using the pressure gradients. In an experimental apparatus, where the problem is transient, this measure can be obtained by using pressure transducers at two near points. This procedure can determine the velocity of the propagating front and the two pressure gradients of the fully developed regions.

The main numerical result obtained was a construction of a map in the space formed by ($Ca \times N_\mu$), where it is easy to locate the different flow regimes of the problem. Therefore, different paths in this space can be followed from one case to another. Concerning the flow regimes, we have found that the effects of the capillary number and viscosity ratio are in the same direction: increasing Ca or N_μ, we increase the tendency of the flow to have a bypass pattern. The reason for this seems to be related to the ratio of the dimensionless numbers that appears in the tangential (N_μ) and normal (N_σ) balance of forces at the interface in Region IV, $N_\mu/N_\sigma = N_\mu Ca(1-m)(\mathrm{d}p*/\mathrm{d}x_I)$, where there is a similar dependence on a change of Ca or N_μ. The dimensionless numbers N_μ and N_σ can also be used to explain the relation between viscoelasticity and interfacial forces and the competition between elasticity and pseudo-plastic effects, since in a Newtonian–viscoelastic displacement there is another stress jump in Region IV due to the first normal stress difference in shear.

A refinement in the conditions near the transition between the regimes was done to locate the critical conditions. In order to give the streamline patterns, different meshes were used, refined at different locations, by changing the pressure level at the inlet.

Figures 8–10 and the qualitative sketch in figure 11 show that the transition window is narrow and, therefore, difficult to be captured, specially in an experimental investigation. We hope that these results can be used to guide experimental and numerical work for the precise location of the critical conditions.

The authors are grateful to Professor Angelo Rangel who read an early version of the paper and contributed with valuable comments and suggestions. The authors also acknowledge the referees for a great number of suggestions that improved the quality of the final text. This research was partially funded by grants from Conselho Nacional de Pesquisa e Desenvolvimento (CNPq), Agência Nacional de Petróleo (ANP), PETROBRAS and Fundação de Amparo à Pesquisa do Rio de Janeiro (FAPERJ).

REFERENCES

Allouche, M., Frigaard, I. A. & Sona, G. 2000 Static wall layers in the displacement in two visco-plastic fluids in a plane channel. *J. Fluid Mech.* **424**, 243–277.

Bretherton, F. P. 1961 The motion of long bubble in tubes. *J. Fluid Mech.* **10**, 166–188.

Christodoulou, K. N. & Scriven, L. E. 1992 Discretization of free surface flows and other moving boundary. *J. Comput. Phys.* **99**, 39–55.

Cox, B. G. 1962 On driving a viscous fluid out of a tube. *J. Fluid Mech.* **20**, 81–96.

Dimakopoulos, Y. & Tsamopoulos, J. 2003*a* A quasi-elliptic transformation for moving boundary problems with large anisotropic deformations. *J. Comput. Phys.* **192**, 494–522.

Dimakopoulos, Y. & Tsamopoulos, J. 2003*b* Transient displacement of a viscoplastic material by air in straight and constricted tubes. *J. Non-Newton. Fluid Mech.* **112**, 43–75.

Dimakopoulos, Y. & Tsamopoulos, J. 2004 On the gas-penetration in straight tubes completely filled with a viscoelastic fluid. *J. Non-Newton. Fluid Mech.* **117**, 117–139.

Dimakopoulos, Y. & Tsamopoulos, J. 2007 Transient displacement of newtonian and viscoplastic liquids by air in complex tubes. *J. Non-Newton. Fluid Mech.* **142**, 162–182.

Fairbrother, F. & Stubbs, A. E. 1935 Studies in electro-endosmosis. Part VI. The 'bubble-tube' method of measurement. *J. Chem. Soc.* **1**, 527–539.

Goldsmith, H. L. & Mason, S. G. 1963 The flow of suspensions through tubes. *J. Colloid Sci.* **18**, 237–261.

Hodges, S. R., Jenseng, O. E. & Rallison, J. M. 2004 The motion of a viscous drop through a cylindrical tube. *J. Fluid Mech.* **501**, 279–301.

Huen, C. K., Frigaard, I. A. & Martinez, D. M. 2007 Experimental studies of multi-layer flows using a visco-plastic lubricant. *J. Non-Newton. Fluid Mech.* **142**, 150–161.

Huzyak, M. & Koelling, I. A. 1997 The penetration of a long bubble through a viscoelastic fluid in a tube. *J. Non-Newton. Fluid Mech.* **71**, 73–88.

Lac, E. & Sherwood, J. D. 2009 Motion of a drop along the centreline of a capillary in a pressure-driven flow. *J. Fluid Mech.* **640**, 27–54.

Lee, G., Shaqfeh, E. S. G. & Khomami, B. 2002 A study of viscoelastic free surface by finite element method Hele–Shaw and slot coating flows. *J. Non-Newton. Fluid Mech.* **117**, 117–139.

Martinez, M. J. & Udell, K. S. 1990 Axisymmetric creeping motion of drops through circular tubes. *J. Fluid Mech.* **210**, 565–591.

Poslinski, A. J., Oehler, P. O. & Stokes, V. K. 1995 Isothermal gas-assisted displacement of a viscoplastic liquid in tubes. *Polym. Engng Sci.* **35**, 877–892.

Sackinger, P. A., Shunk, P. R. & Rao, R. R. 1996 A Newton–Rhaphson pseudo-solid domain mapping technique for free and moving boundary problems: a finite element implementation. *J. Comput. Phys.* **125**, 83–103.

Soares, E. J., Carvalho, M. S. & de Souza Mendes, P. R. 2005 Immiscible liquid–liquid displacement in capillary tubes. *J. Fluids Engng* **127**, 24–31.

Soares, E. J., Carvalho, M. S. & de Souza Mendes, P. R. 2006 Gas-displacement of non-newtonian liquids in capillary tubes. *Intl J. Heat Fluid Flow* **27**, 95–104.

Soares, E. J., Carvalho, M. S. & de Souza Mendes, P. R. 2008 Immiscible liquid–liquid displacement in capillary tubes: viscoelastic effects. *J. Braz. Soc. Mech. Sci. Engng* **27**, 160–165.

Sousa, D. A., Soares, E. J., Queiroz, R. S. & Thompson, R. L. 2007 Numerical investigation on gas-displacement of a shear-thinning liquid and a visco-plastic material in capillary tubes. *J. Non-Newton. Fluid Mech.* **144**, 149–159.

Sousa, R. G., Pinto, A. M. F. R & Campos, J. B. L. M. 2006 Effect of gas expansion on the velocity of a taylor bubble: PIV measurements. *Intl J. Multiphase flow* **32**, 1182–1190.

de Souza Mendes, P. R., Dutra, E. S. S., Siffert, J. R. R. & Naccache, M. F. 2007 Gas displacement of viscoplastic liquids in capillary tubes. *J. Non-Newton. Fluid Mech.* **145**, 30–40.

Taylor, G. I. 1961 Deposition of a viscous fluid on the wall of a tube. *J. Fluid Mech.* **10**, 161–165.

Westborg, H. & Hassager, O. 1989 Creeping motion of long bubbles and drops in capillary tubes. *J. Colloid Interface Sci.* **133**, 135–147.